Spectrochimica Acta Part A: Molecular and Biomolecular Spectroscopy 97 (2012) 683–694

Contents lists available at SciVerse ScienceDirect

Spectrochimica Acta Part A: Molecular and Biomolecular Spectroscopy

journal homepage: www.elsevier.com/locate/saa

Co(II), Cd(II), Hg(II) and U(VI)O_2 complexes of *o*-hydroxyacetophenone[*N*-(3-hydroxy-2-naphthoyl)] hydrazone: Physicochemical study, thermal studies and antimicrobial activity

R.R. Zaky [a], T.A. Yousef [b,*], K.M. Ibrahim [a]

[a] Department of Chemistry, Faculty of Science, Mansoura University, Mansoura, Egypt
[b] Department of Toxic and Narcotic Drug, Forensic Medicine, Mansoura Laboratory, Medicolegal Organization, Ministry of Justice, Egypt

HIGHLIGHTS

- Synthesis of *o*-hydroxy acetophenone [*N*-(3-hydroxy-2-naphthoyl)] hydrazone.
- Synthesis and characterization Co(II), Cd(II), Hg(II) and U(VI)O_2 complexes with hydrazone.
- Kinetic parameters (*Ea*, *A*, ΔH, ΔS and ΔG) have been calculated.
- Molecular modeling of the free ligand and its complexes has been calculated.
- Antibacterial and antifungal studies showing good results.

GRAPHICAL ABSTRACT

Effect of ligand and its metal complexes toward (A) *Aspergillus* sp., (B) *Stemphylium* sp. and (C) *Trichoderma* sp.

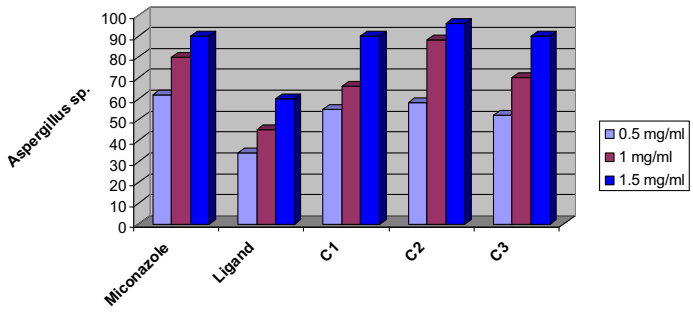

ARTICLE INFO

Article history:
Received 28 March 2012
Received in revised form 4 May 2012
Accepted 17 May 2012
Available online 4 July 2012

Keywords:
Hydrazone complexes
^{1}H and ^{13}C NMR
Thermal analysis
Antibacterial and antifungal activity

ABSTRACT

The *o*-Hydroxy acetophenone [*N*-(3-hydroxy-2-naphthoyl)] hydrazone (H_2o-HAHNH) has been prepared and its structure is confirmed by elemental analysis, IR, ^{1}H NMR and ^{13}C NMR spectroscopy. It has been used to produce diverse complexes with Co(II), Cd(II), Hg(II) and U(VI)O_2 ions. The isolated complexes have been investigated by elemental analysis, magnetic measurements, molar conductivity, thermal (TG, DTG) and spectral (^{1}H NMR, ^{13}C NMR, IR, UV–visible, MS) studies. Infrared spectra suggested H_2o-HAHNH acts as a bidentate and/or tridentate ligand. The electronic spectrum of [Co(H*o*-HAHNH)$_2$] complex as well as its magnetic moments suggesting octahedral geometry around Co(II) center. The TG analyses suggest high stability for most complexes followed by thermal decomposition in different steps. Moreover, the kinetic and thermodynamic parameters (*Ea*, *A*, ΔH^*, ΔS^* and ΔG^*) for the different decomposition steps of the [Co(H*o*-HAHNH)$_2$] and [Cd(H*o*-HAHNH)$_2$] complexes were calculated using the Coats–Redfern and Horowitz–Metzger methods. Moreover, the antibacterial and antifungal activities of the isolated compounds were studied using a wide spectrum of bacterial and fungal strains.

Introduction

Schiff bases hydrazone derivatives and their metal complexes have been studied for their interesting and important properties, e.g., antibacterial [1,2], antifungal [3]. Schiff bases hydrazone derivatives are versatile ligands and they offer the possibility of different modes of coordination towards transition metal ions.

* Corresponding author at: Department of Chemistry, Faculty of Science, Mansoura University, Mansoura, Egypt. Tel.: +20 1222247712.
E-mail address: drroka78@yahoo.com (T.A. Yousef).

1386-1425/$ - see front matter © 2012 Elsevier B.V. All rights reserved.
http://dx.doi.org/10.1016/j.saa.2012.05.086

They also employ as extracting agents in spectrophotometric determination of some ions [4] and spectrophotometric determination of some species in pharmaceutical formulations [5], as well as uses in catalytic processes [6,7] and wastewater treatment [8]. We have recently published some transition metal complexes of hydrazones derived from 3-hydroxy naphthoic acid hydrazide [9–11]. In continuation of our previous work on hydrazones [1,2], the present work aims to synthesize and characterize complexes of *o*-hydroxyacetophenone [*N*-(3-hydroxy-2-naphthoyl)] hydrazone (H_2*o*-HAHNH) with Co(II), Cd(II), Hg(II) and U(VI)O_2 ions. The possible modes of chelations, the geometry and the nature of bonding of the complexes are discussed based on various spectroscopic methods (^{1}H NMR, ^{13}C NMR, IR, UV–visible, MS). In addition, the kinetics and thermodynamic parameters of the decomposition steps for Co(II) and Cd(II) complexes have been studied employing Coats–Redfern and Horowitz–Metzger methods. The antibacterial and antifungal activities of the ligand and its metal complexes have also been examined.

Experiment

Material

All manipulations were performed under aerobic conditions. All metal salts and other reagents used were pure (Fluka, Aldrich or Merck).

Preparation of o-Hydroxy acetophenone [N-(3-hydroxy-2-naphthoyl)] hydrazone (H_2*o*-HAHNH, $C_{19}H_{16}O_3N_2$)

H_2*o*-HAHNH (Scheme 1) was prepared by heating a mixture of 3-hydroxy naphthoic acid hydrazide (0.01 mol; 2.02 g) and *o*-hydroxy acetophenone (0.01 mol; 1.36 g) under reflux in absolute ethanol for 2 h. On heating, pale yellow crystals were formed, filtered off, washed with absolute ethanol and diethyl ether, and recrystallized from EtOH (M.p.: 290 °C; yield 90%). The purity of the compound was checked by TLC.

Synthesis of metal complexes

The metal complexes were synthesized by taking 50 ml solutions of each Co(II), Cd(II), Hg(II) and U(VI)O_2 acetate (10 mmol) in distilled water or absolute ethanol and 50 ml hot absolute ethanol solution of the ligand H_2*o*-HAHNH (10 mmol, 3.20 g) in a round-bottom flask. After refluxing the reactants for 1–3 h and cooling to room temperature, the complexes precipitated and were filtered in a glass crucible. The products were washed several times with water, ethanol and finally with diethyl ether and the pure complexes thus obtained were dried in a desiccator over anhydrous $CaCl_2$. The isolated complexes are powder-like, stable in the normal laboratory atmosphere, and soluble in DMF or DMSO. The characterization of these complexes was based on the physical and spectroscopic techniques.

Analyses of the complexes

Elemental analyses

The complexes were analyzed for metal content gravimetrically by literature procedures [12] after decomposing the organic matter with a mixture of HNO_3 and HCl and evaporating from the residue to dryness with concentrated H_2SO_4.

Physico-chemical measurements

Elemental analyses (C and H) were performed on a Perkin–Elmer 2400 Series II Analyzer. The molar conductance of the complexes were determined by preparing 10^{-3} M solutions of the complexes in DMSO at room temperature and measured on a YSI Model 32 conductivity bridge. Thermogravimetric analysis was performed using an automatic recording thermobalance type (DuPont 951 Instrument) Thermal Analyzer between room temperature to 800 °C. Magnetic moment values were evaluated at room temperature (25 ± 1 °C) using a Johnson Matthey magnetic susceptibility balance using Hg[Co(SCN)$_4$] as calibrant. The electronic spectrum of Co(II) complex was recorded in DMSO solution on an Unicam UV_2–UV–visible spectrometer, in the range 200–900 nm. Infrared spectra of the ligand and its metal complexes were recorded on Mattson 5000 FTIR spectrophotometer, in the range 4000–500 cm^{-1} in KBr disk. Mass spectra were recorded on a Mattson 5000 FTIR spectrophotometer. ^{1}H and ^{13}C NMR spectra of the ligand and Cd(II), Hg(II) and U(VI)O_2 complexes were recorded in DMSO on an EM-390 (200 MHz) spectrometer.

Molecular modeling

An attempt to gain better insight on the molecular structure of the ligand and its complexes, geometric optimization and conformational analysis has been performed using PM3 [13] forcefield as implemented in hyperchem 8 [14]. The low lying obtained from MM+ was then optimized at PM3 using the Polak–Ribiere algorithm in RHF-SCF, set to terminate at an RMS gradient of 0.01 kcal mol^{-1}.

Biological activity

Antifungal activity

Antifungal activity, based on the determined growth inhibition rates of the mycelia of strain (*Aspergillus* sp., *Trichoderma* sp. and *Stemphylium* sp.) in Potato Dextrose Broth medium (PDB) were determined. These species were isolated from the infected organs of the host plants on potato dextrose agar (potato 250 g + dextrose 20 g + agar 20 g) medium. The cultures of the fungi were purified by single spore isolation technique. The solution in different concentrations 0.5, 1 and 1.5 mg/ml of each compound in DMSO were prepared for testing against spore germination. A drop of the solution of each concentration was kept separately on glass slides. The conidia, fungal reproducing spores (approximately 200) lifted with the help of an inoculating needle, were mixed in every drop of each compound separately. Each treatment was replicated thrice and a parallel DMSO solvent control set was run concurrently on separate glass slides. All the slides were incubated in humid chambers at 25 ± 2 °C for 24 h. Each slide was observed under the microscope for spore germination and percent germination was finally calculated. A zone of inhibition of growth was taken as an indication of antifungal activity. The results were also compared with a standard antifungal drug Miconazole at the same concentrations.

Antibacterial activity

Chemical compounds were individually tested against a panel of gram positive *Clostridium* sp. and negative *Escherichia coli* bacterial pathogens. Each of the compounds was dissolved in DMSO and solutions of the concentration 2 mg/ml and 1 mg/ml were prepared separately. Paper discs of Whatman filter paper were prepared with standard size (5 cm) were cut and sterilized in an autoclave. The paper discs soaked in the desired concentration of the complex solutions were placed aseptically in the petridishes containing nutrient agar media (agar 20 g + beef extract 3 g + peptone 5 g) seeded with *Clostridium* sp. and *E. coli* bacteria separately. The petridishes were incubated at 37 °C and the inhibition zones were recorded after 24 h of incubation. Each treatment was replicated nine times. The antibacterial activity of a common standard antibiotic ampicillin was also recorded using the same procedure

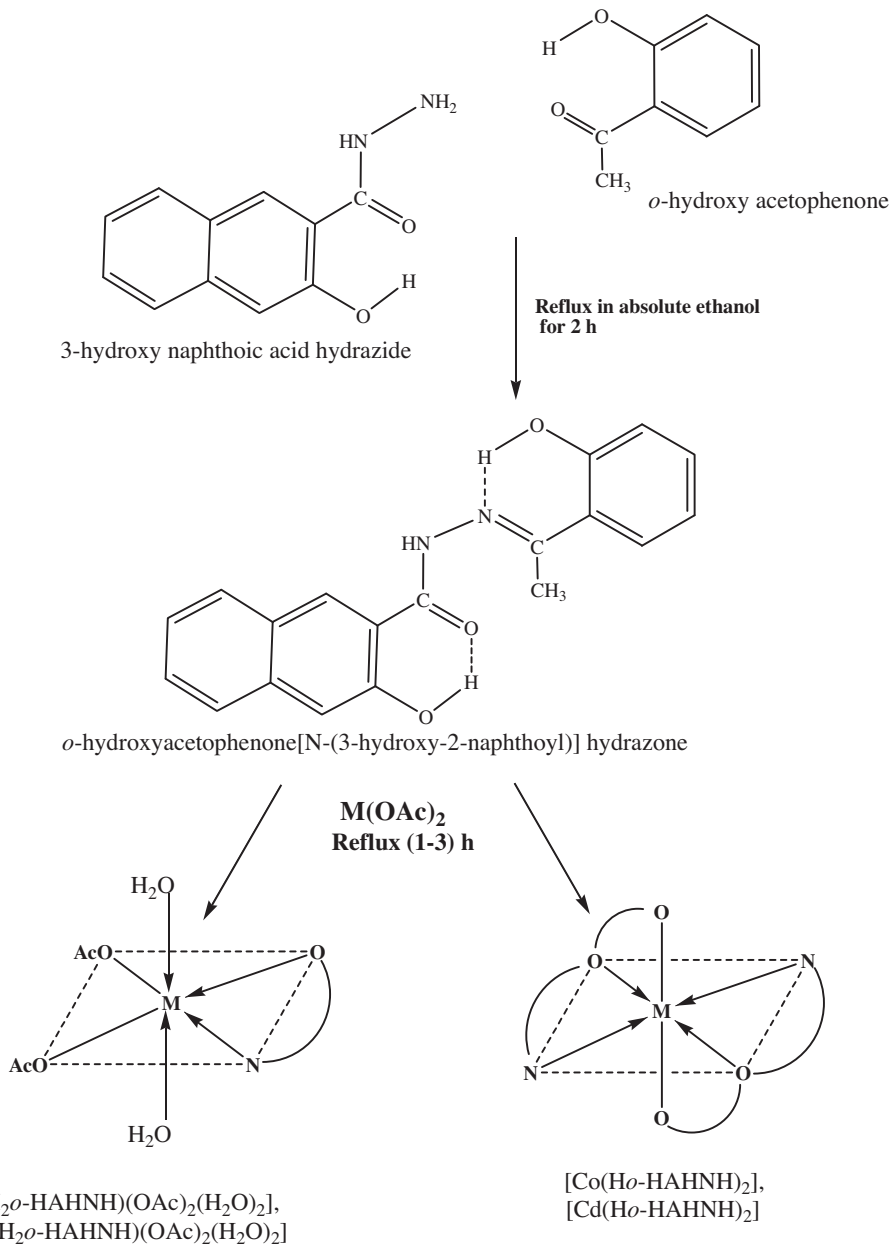

Scheme 1. The outline of the synthesis of ligand and its complexes.

as above at the same concentrations and solvent. The % Activity Index for the complex was calculated by the formula as under:

$$\%\text{Activity Index} = \frac{\text{Zone of inhibition by test compound(diametre)}}{\text{Zone of inihibition by standard(diametre)}} \times 100$$

Minimal inhibitory concentration (MIC) measurement

The MIC was determined using the disc diffusion technique by preparing discs containing 0.1–1.0 mg/ml of each compound against both the bacteria and applying the protocol. The twofold dilutions of the solution were prepared. The microorganism suspensions at 10 CFU/ml (colony forming unit/ml) concentration were inoculated to the corresponding wells. The plates were incubated at 36 °C for 24 for the bacteria. At the end of the incubation period, the minimal inhibitory concentrations (MIC) values were recorded as the lowest concentrations of the substance that had no visible turbidity. Control experiments with DMSO and uninoculated media were run parallel to the test compounds under the same conditions. All the compounds were more effective at 1.0 and 2.0 mg/ml concentrations. Consequently, all the compounds were screened at these concentrations against both the bacteria.

Results and discussion

The color, melting points and elemental analyses of the ligand and isolated complexes are listed in Table 1. The isolated solid complexes are stable in the air and easily soluble in DMF and DMSO only. All complexes decompose on heating at >300 °C. The molar conductance values, in DMSO, are 3–7 $Ohm^{-1}cm^2\ mol^{-1}$ indicating that all complexes are non-electrolytes.

IR spectral studies

The infrared spectrum of H_2o-HAHNH displays five bands at 1647, 1618, 3125, 3240 and 3419 cm^{-1} assigned to ν(C=O) [15], ν(C=N)$_{hydrazone}$ [16], ν(NH) [17], (OH)$_{naphthoic}$ [18] and (OH)$_{phenolic}$ [18] vibrations, respectively. The two bands at 1273 and 1365 cm^{-1} are attributed to δ(OH)$_{phenolic}$ and δ(OH)$_{naphthoic}$ [19]. The appearance of (OH)$_{naphthoic}$ and (OH)$_{phenolic}$ as a broad band at lower wavenumbers and the two weak broad bands in the 1900–2080 and 2150–2230 cm^{-1} regions suggest intramolecular hydrogen bonding (O–H···O) [19].

Comparison of the infrared spectrum of the ligand with those of its metal complexes reveals that H_2o-HAHNH (Structure 1) behaves as a bidentate and/or tridentate ligand depending on the metal salt and the reaction conditions (Scheme 1, Table 2).

In [UO_2(H_2o-HAHNH)$(OAc)_2(H_2O)_2$] (Structure 2) and [Hg(H_2o-HAHNH)$(OAc)_2(H_2O)_2$] complexes, H_2o-HAHNH acts as a neutral bidentate ligand coordinating *via* carbonyl oxygen (C=O) and azomethine nitrogen (C=N). This mode of chelation is supported by the shift of both ν(C=N) and ν(C=O) vibrations to lower wavenumber. The ν(NH) vibration remains more or less at the same position. The ν(OH)$_{naphthoic}$ is shifted to higher wavenumber. Moreover, the infrared spectra of these complexes showed new bands at (520, 525) and (425, 432) cm^{-1} assignable to ν(M–O) and ν(M–N), respectively, [20]. The complexes show two bands at (1382, 1376) and (1571, 1573) cm^{-1}, which can be assigned to ν_{as}(O–C–O) and ν_s(O–C–O) of the acetate group. The difference (189, 197 cm^{-1}) between those two bands indicates the monodentate bonding for the acetate group [21]. Also, the bands of coordinated water observed at (824, 844) and (531, 546) cm^{-1}, are assigned to $\rho_r(H_2O)$ and $\rho_w(H_2O)$, respectively, [21]. Moreover, strong evidence for the presence or absence of coordinated water supported by the thermogram of all complexes.

Also, H_2o-HAHNH behaves as a mononegative tridentate ligand coordinating through the azomethine nitrogen (C=N), carbonyl oxygen (C=O) and the (OH)$_{naphthoic}$ with the displacement of the hydrogen atom from the latter group. This behavior is observed in [Co(H*o*-HAHNH)$_2$] (Structure 3) and [Cd(H*o*-HAHNH)$_2$] complexes. This mode of chelation is based on the disappearance of the (OH)$_{naphthoic}$ and the shift of both ν(C=O) and ν(C=N) to lower wavenumbers. In addition, the new bands were observed at (512, 525) and (425, 430) cm^{-1} tentatively attributed to ν(M–O) and ν(M–N), respectively [20].

The infrared spectrum of [UO_2(H_2o-HAHNH)$(OAc)_2(H_2O)_2$] complex displays two bands at 920 and 870 cm^{-1} assigned to ν_3 and ν_1 vibrations, respectively, of the dioxouranium ion. The ν_3 value is used to calculate the force constant (F) of ν(U=O) by the method of McGlynn et al. [22].

$$(\nu_3)^2 = (1307)2(F_{U-O})/14.103$$

The force constant obtained for uranyl complex was then substituted into the relation given by Jones [23] to give an estimate of the (U–O) bond length in Å.

$$R_{U-O} = 1.08(F_{U-O})^{-1/3} + 1.17$$

The calculated F_{U-O} and R_{U-O} values are 6.987 mdynes $Å^{-1}$ and 1.735 Å, respectively, fall in the normal range for the uranyl complexes.

Nuclear magnetic resonance spectral studies

The ^1H and ^{13}C NMR spectra of H_2o-HAHNH and its Cd(II), Hg(II) and U(VI)O_2 complexes (Scheme 2) were recorded in DMSO. The ^1H NMR spectrum of H_2o-HAHNH in DMSO shows three signals at 11.24, 11.32 and 12.19 ppm assignable to the protons of (NH), (OH)$_{phenolic}$ and (OH)$_{naphthoic}$ respectively (Table 3). The appearance of the signal attributed to the proton of OH group at a high value downfield from TMS suggests the presence of intramolecular hydrogen bonding. The multiplet signals observed in the 6.92–8.67 ppm region are assigned to the aromatic protons. Also, the ^1H NMR spectra of the Hg(II) and U(VI)O_2 complexes show the signals attributed to the (NH), (OH)$_{naphthoic}$ and (OH)$_{phenolic}$ protons remain more or less at the same positions indicating that these groups play no part in coordination but in case of ^1H NMR spectrum of Cd(II) complex there is no signal attributable to (OH)$_{naphthoic}$ proton indicating the deprotonation of this group on complexation. The most significant features of the ^{13}C NMR spectra of the Hg(II), U(VI)O_2, Cd(II) complex were detected when comparing with the spectrum of the corresponding free ligand. From ^{13}C NMR spectral data (Table 4), for the Hg(II) and U(VI)O_2 complexes, the signal for C_3 and C_4 carbon showed an upfield shift on complexation [24] compared with the free ligand. Moreover, the appearance of new signals at (174, 177) and (52, 55) ppm give strong evidence for the presence of the acetate group. Additionally, the signal for C_3 and C_4 carbon of Cd(II) complex showed an upfield shift while, C_6 showed an downfield shift on complexation. The other ring carbon atoms did not show significant shifts.

Electronic spectra

The electronic spectrum of [Co(H*o*-HAHNH)$_2$] complex shows two bands at 14,211 and 17,212 cm^{-1} attributed to $^4T_{1g}(F) \rightarrow {}^4A_{2g}(F)$ and $^4T_{1g}(F) \rightarrow {}^4T_{1g}(P)$ transitions, respectively, in an octahedral configuration [25]. The calculated values of D_q (766), B (766), β (0.76) and ν_2/ν_1 (2.15) are in good agreement with those reported for octahedral Co(II) complexes. In addition, the magnetic moment (4.98 BM) is consistent with octahedral geometry around the Co(II) ion.

The electronic spectrum of [UO_2(H_2o-HAHNH)$(OAc)_2(H_2O)_2$] complex contains two bands at 21,276 and 25,000 cm^{-1} may be attributed to $^1\sum_g^+ \rightarrow {}^2\pi_u$ transition and charge transfer $n \rightarrow \pi^*$, respectively [25].

Table 1
Analytical and physical data of H_2o-HAHNH and its metal complexes.

Compound Empirical Formula F.W. Found (Calcd.)	Color	Yield (%)	%Found (Calcd.) C	H	M
H_2o-HAHNH $C_{19}H_{16}O_3N_2$ 320.112 (320.350)	Yellow	90	71.24 (71.27)	5.08 (5.03)	
[Co(H*o*-HAHNH)$_2$] **(C1)** $CoC_{38}H_{30}O_6N_4$ 696.841 (697.617)	Brown	85	65.48 (65.42)	4.40 (4.33)	8.46 (8.54)
[Cd(H*o*-HAHNH)$_2$] **(C2)** $CdC_{38}H_{30}O_6N_4$ 751.968 (751.070)	Yellowish-white	78	60.54 (60.76)	4.12 (4.02)	14.42 (14.90)
[UO_2(H_2o-HAHNH)$(OAc)_2(H_2O)_2$] **(C3)** $UC_{23}H_{26}O_{11}N_2$ 745.351 (744.411)	Orange	80	37.22 (37.10)	3.49 (3.52)	32.07 (31.90)
[Hg(H_2o-HAHNH)$(OAc)_2(H_2O)_2$] **(C4)** $HgC_{23}H_{26}O_9N_2$ 674.751 (675.011)	Yellowish-white	75	40.87 (40.93)	3.98 (3.88)	29.86 (29.70)

In *DMSO* (ohm^{-1} cm^2 mol^{-1}).

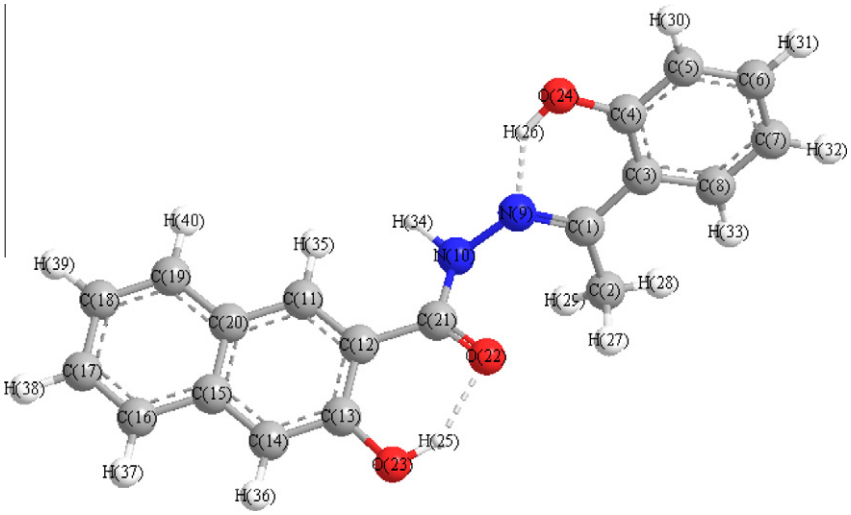

Structure 1. Molecular modelling of H_2o-HAHNH.

Table 2
Most important IR spectral bands of H_2o-HAHNH and its metal complexes in cm^{-1}.

Compound	$\upsilon(OH)_{naphthoic}$	$\upsilon(OH)_{phenolic}$	$\upsilon(NH)$	$\upsilon(C{=}O)$	$\upsilon(C{=}N)$	$\upsilon(C{-}O)_{naphthoic}$	$\upsilon(M{-}O)$	$\upsilon(M{-}N)$
H_2o-HAHNH	3240	3419	3125	1647	1618	1219	–	–
$[UO_2(H_2o\text{-HAHNH})(OAc)_2(H_2O)_2]$	3305	3425	3189	1630	1596	1246	520	425
$[Hg(H_2o\text{-HAHNH})(OAc)_2(H_2O)_2]$	3445	3430	3186	1629	1598	1233	511	420
$[Co(Ho\text{-HAHNH})_2]$	-	3445	3223	1633	1597	1234	525	430
$[Cd(Ho\text{-HAHNH})_2]$	-	3430	3221	1631	1598	1236	512	425

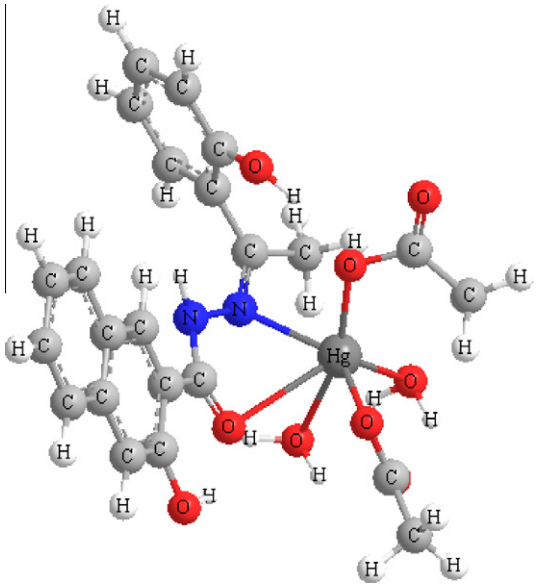

Structure 2. Molecular modelling of $[Hg(H_2o\text{-HAHNH})(OAc)_2(H_2O)_2]$ complex.

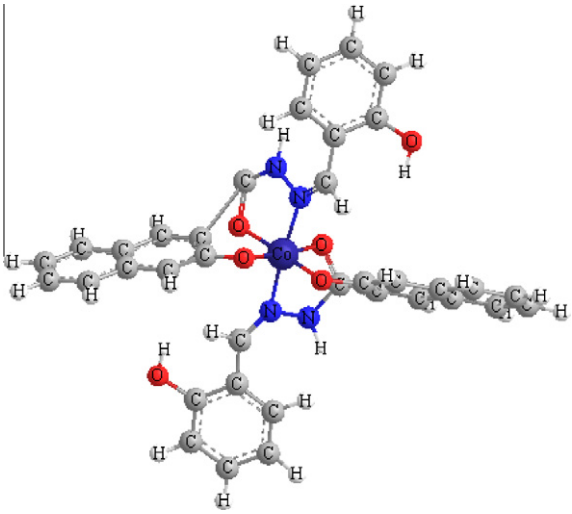

Structure 3. Molecular modelling of $[Co(Ho\text{-HAHNH})_2]$ complex.

Molecular modeling

The atomic numbering scheme and the theoretical geometry structures for the ligand and some of its metal complexes are calculated. The molecular parameters: total energy, binding energy, isolated atomic energy, electronic energy, heat of formation, dipole moment, HOMO and LUMO were calculated and represented in Table 5. A comparison between the bond length of the ligand and its complexes is illustrated. All the active groups taking part in coordination have bonds longer than that already exist in the ligand (like C=N, O–H, and C=O). The lower HOMO energy values show that molecule donating electron ability is the weaker. On contrary, the higher HOMO energy implies that the molecule is a good electron donor. LUMO energy presents the ability of a molecule receiving electron [26].

Thermal analysis

The TG and DTG curves of $[Co(Ho\text{-HAHNH})_2]$ complex show that it is thermally stable up to 365 °C, above which point partial decomposition of the complex begins. In the temperature range 365–450 °C, the TG curve is indicative of 26.6% weight loss, which

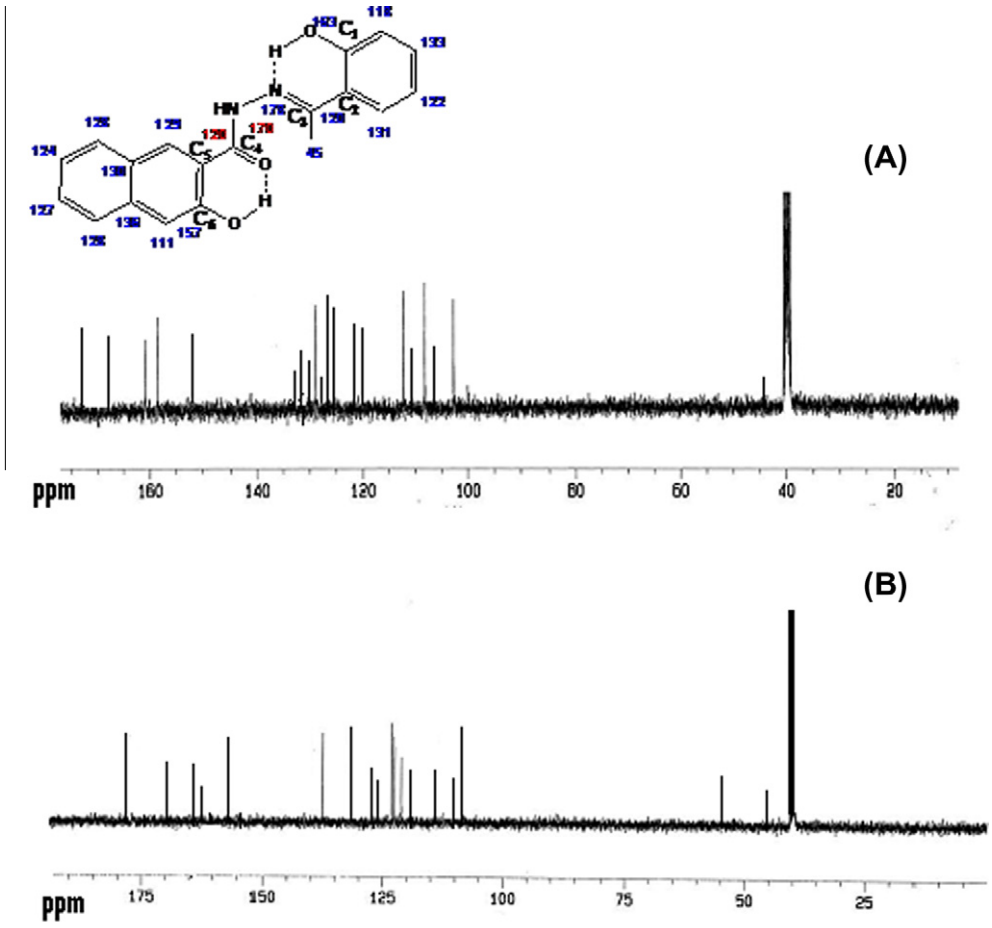

Scheme 2. ^{13}C NMR spectra of (A) H_2o-HAHNH and (B) $[Hg(H_2o\text{-}HAHNH)(OAc)_2(H_2O)_2]$ complex.

Table 3
The ^1H NMR spectral data of H_2o-HAHNH and its diamagnetic complexes.

Compounds	$-CH_3$	Aromatic protons	NH	$(OH)_{phenolic}$	$(OH)_{naphthoic}$
H_2o-HAHNH	1.88	6.92–8.67	11.24	11.32	12.19
$[Cd(Ho\text{-}HAHNH)_2]$	1.83	6.98–8.69	11.36	11.45	–
$[UO_2(H_2o\text{-}HAHNH)(OAc)_2(H_2O)_2]$	1.91	7.11–8.66	11.27	11.41	12.21
$[Hg(H_2o\text{-}HAHNH)(OAc)_2(H_2O)_2]$	1.90	7.11–8.72	11.31	11.44	12.17

Table 4
^{13}C NMR Chemical shifts in (ppm) assignments for H_2o-HAHNH and its diamagnetic complexes.

Compound	C_1	C_2	C_3	C_4	C_5	C_6
H_2o-HAHNH	163	120	178	170	120	157
$[Cd(Ho\text{-}HAHNH)_2]$	164	121	169	163	130	162
$[UO_2(H_2o\text{-}HAHNH)(OAc)_2(H_2O)_2]$	163	119	171	165	126	158
$[Hg(H_2o\text{-}HAHNH)(OAc)_2(H_2O)_2]$	164	120	170	165	127	156

could be ascribed to the elimination of the two loosely bound 3-hydroxynaphthoyl ($2C_6H_5O$) moieties. The second weight loss stage (450–640 °C) is largely due to the full decomposition of the remaining organic portions ($2C_{13}H_{10}N_2$) of the two ligand molecules and release half an oxygen molecule. This stage is accompanied by 62.7% weight loss in the TG curve. The remaining final fired product is CoO representing 10.7% (Scheme 3).

The $[Cd(Ho\text{-}HAHNH)_2]$ complex is thermally stable up to 335 °C above which point partial decomposition begins. In the temperature range 335–460 °C, the TG curve exhibit 24.8% weight loss which could be ascribed to the elimination of ($2C_6H_5O$) moieties. The second weight loss stage (460–565 °C) is largely due to the full decomposition of the remaining organic portions ($2C_{13}H_{10}N_2$) of the two ligand molecules as well as the release of half oxygen molecule. This stage is accompanied by 58.1% weight loss in the TG curve. The remaining final fired product is CdO, representing 17.1%.

Kinetic data

Non-isothermal calculations were used extensively to evaluate the thermodynamic and kinetic parameters for the different thermal decomposition steps of the Co(II) complexes were determined using the Coats–Redfern [27] and Horowitz–Metzger [28].

The rate of decomposition of a solid depends upon the temperature and the amount of material. The expression for the thermal decomposition of a homogeneous system has the following general form:

$$\frac{d\alpha}{dt} = K(T)g(\alpha) \quad (1)$$

Where t is the time, T is the absolute temperature and α is the degree of transformation defined as:

$$\alpha = \frac{w_o - w_t}{w_o - w_\infty}$$

In which w_o, w_t and w_∞ are the weights of the sample before the degradation, at temperature t and after total conversion, respectively. $K(T)$ is the rate coefficient that usually follows the Arrhenius equation. The differential conversion function, $g(\alpha)$ may present various functional forms but its most commonly form for solid–state reactions is $g(\alpha) = (1-\alpha)n$, where n is the reaction order, assumed to remain constant during the reaction [29,30].

The rate constant is normally expressed by the Arrhenius equation:

$$K = A\exp\left(-\frac{E_a}{RT}\right) \quad (2)$$

Where Ea is the activation energy, A is the Arrhenius pre-exponential factor which indicates how fast the reaction occurs and R is the gas constant in (J mol^{-1} K). Substituting in Eq. (1), we get:

$$\frac{d\alpha}{dt} = A\exp\left(-\frac{E_a}{RT}\right)g(\alpha) \quad (3)$$

When the reaction is carried out under a linear temperature program ($T = T_o + \beta_t$, where $\beta = dT/dt$ is the heating rate and T_o the starting temperature). A large number of decomposition processes can be represented as first order reaction [31]. Particularly, the degradation of the investigated series of metal complexes was suggested to be first order in sample weight reaction. Therefore we will assume $n = 1$ for the remainder of the present text. Under this assumption the integration of Eq. (3) leads to:

$$\ln(1-\alpha) = -\frac{A}{\beta}\int_{T_o}^{T}\mathrm{Exp}\left(-\frac{E}{RT}\right)dT \quad (4)$$

On the basis of Eq. (4), it is possible to analyze experimental data by the integral method, in order to determine the degradation kinetic parameters A and Ea. The temperature integral in the right-hand side of Eq. (4) has no exact analytical solutions and several kinds of approximations are generally used. Two methods that differ on the way of resolving Eq. (4) are compared using the TGA data of the studied complexes. These methods are

Coats–Redfern method

The Coats–Redfern [27] method is as follows:

$$\ln\left[\frac{g(\alpha)}{T^2}\right] = \ln\left(\frac{AR}{\beta E}\right) - \frac{Ea}{RT} \quad (5)$$

Where $g(\alpha) = 1\text{-}(1-\alpha)1-n/1-n$ for $n \neq 1$ and $g(\alpha) = -\ln(1-\alpha)$ for $n = 1$, R is the universal gas constant. The correlation coefficient, r, was computed using the least square's method for different values of n ($n = 0.33$, 0.5, 0.66 and $n = 1$) by plotting $\ln\left[\frac{g(\alpha)}{T^2}\right]$ versus $1/T$ for the investigated metal complexes are shown in Figs. 1 and 2. The n-value which gave the best fit ($r \approx 1$) was chosen as the order parameter for the decomposition stage of interest. The slope of the straight line equal (Ea/R) and the intercept the pre- exponential factor, A can be determined. The data obtained are represented in Table 6.

Horowitz–Metzger method

The Horowitz–Metzger [28] relation was used to evaluate the degradation kinetics is

Table 5
The molecular parameters of the ligand and its complexes.

The assignment of the theoretical parameters	The compound investigated	The theoretical data
Total energy	H_2o-HAHNH	−85364.0706966 (kcal/mol)
Total energy		−136.036288981 (a.u.)
Binding energy		−4517.0013846 (kcal/mol)
Isolated atomic energy		−80847.0693120 (kcal/mol)
Electronic energy		−619217.2816306(kcal/mol)
Core–core interaction		533853.2109341(kcal/mol)
Heat of Formation		−31.7823846 (kcal/mol)
Dipole moment		2.65 (Debys)
HOMO		−8.810811
LUMO		−1.089322
Total energy	[Co(Ho-HAHNH)$_2$]	−181373.9200668 (kcal/mol)
Total energy		−289.037704065 (a.u.)
Binding energy		−8686.6488648 (kcal/mol)
Isolated atomic energy		−172687.2712020 (kcal/mol)
Electronic energy		−1953127.7461738 (kcal/mol)
Core–core interaction		−42.3760279 (kcal/mol)
Heat of formation		−268.2028648 (kcal/mol)
Dipole moment		3.315 (Debys)
HOMO		−3.84974
LUMO		−1.039509
Total energy	[Hg(H_2o-HAHNH)$(OAc)_2(H_2O)_2$]	−141239.1015403 (kcal/mol)
Total energy		−225.078807463 (a.u.)
Binding energy		−6415.4095063 (kcal/mol)
Isolated atomic energy		−134823.6920340 (kcal/mol)
Electronic energy		−1301268.8363412 (kcal/mol)
Core–core Interaction		1160029.7348009 (kcal/mol)
Heat of formation		−353.5665063 (kcal/mol)
Dipole moment		8.044 (Debys)
HOMO		−5.868872
LUMO		−1.131408

$$\ln[-\ln(1-\alpha)] = \frac{Ea\theta}{RT_s^2} \qquad \text{For } n = 1 \quad (6)$$

$$\ln\left[\frac{1-(1-\alpha)^{1-n}}{1-n}\right] = \ln\left(\frac{A}{\beta}\frac{RT_S^2}{E}\right) - \frac{E_a}{RT_S} + \frac{E_a\theta}{RT_S^2} \qquad \text{For } n \neq 1 \quad (7)$$

Where $\theta = T\text{–}T_s$, T_s is the DTG peak temperature, T the temperature corresponding to weight loss Wt. In this method a straight line should be observed between $\ln v[-\ln(1-\alpha)]$ and θ with a slope of $\frac{Ea}{RT_s^2}$.

Figs. 3 and 4 show the Horowitz–Metzger plots for the metal complexes under study. The obtained data are recorded in Table 7.

Thermodynamic parameters

The other thermodynamic parameters of activation can be calculated by Eyring equation [32,33]:

$$\Delta H^* = Ea - RT \quad (8)$$

$$\Delta S^* = R\left(\ln\frac{hA}{k_B T} - 1\right) \quad (9)$$

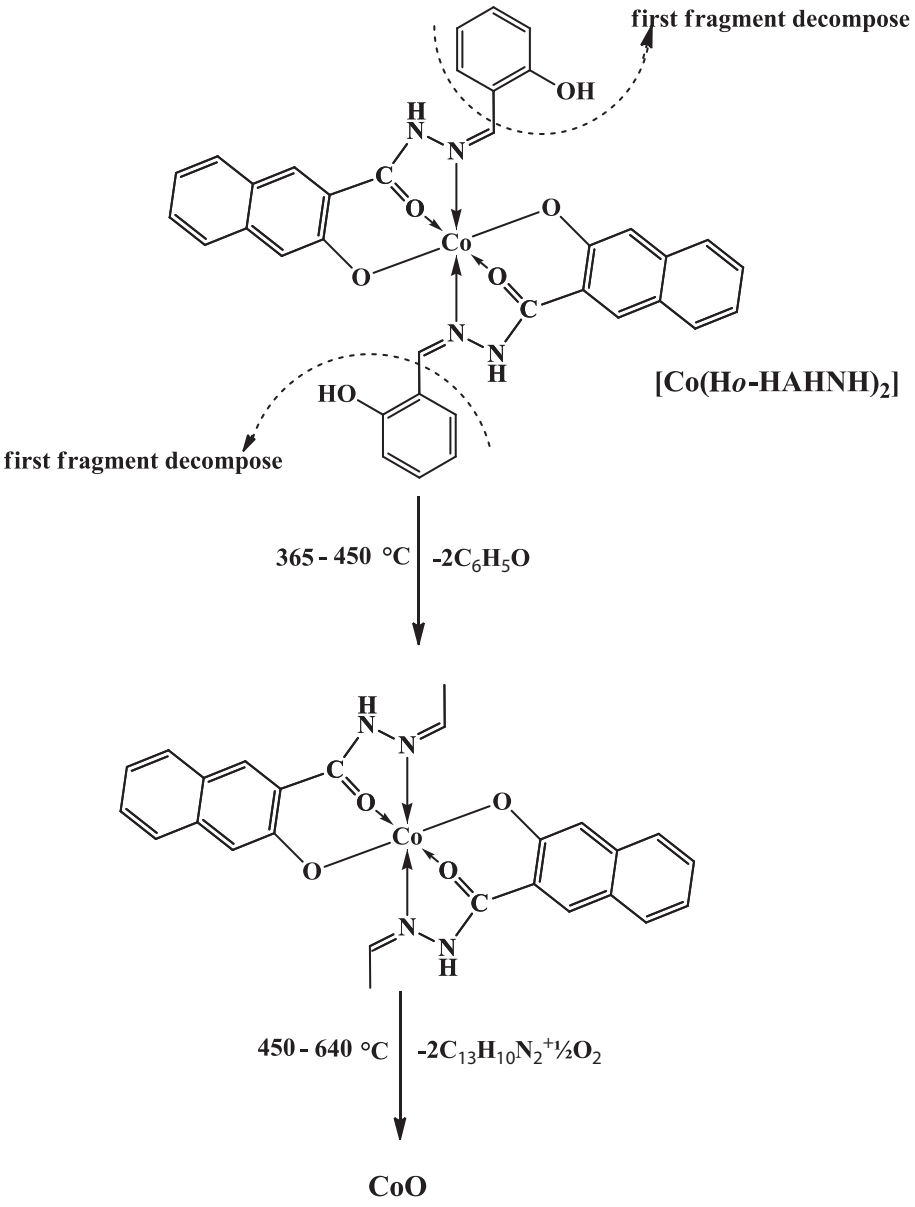

Scheme 3. Decomposition pathway of [Co(Ho-HAHNH)$_2$] complex.

$$\Delta G^* = \Delta H - T\Delta S \quad (10)$$

Where ΔH^* is the enthalpy of activation (kJ/mol), ΔS^* is the entropy of activation (kJ/mol.K) and ΔG^* is the Gibbs free enthalpy of activation (kJ/mol), h is the Planck constant and k_B the Boltzmann constant. The kinetic parameters evaluated by Coats–Redfern and Horowitz–Metzger methods are listed in Tables 6 and 7, respectively. From the results the following remarks can be pointed out:

(i) The kinetic parameters (*Ea*, *A*, ΔH^*, ΔS^* and ΔG^*) of all studied complexes have been determined (Tables 6 and 7) using CR and HM methods. The values obtained from the two methods are quite comparable.
(ii) The thermodynamic data obtained with the two methods are in harmony with each other.
(iii) The correlation coefficients of the Arrhenius plots of the thermal decomposition steps were found to lie in the range 0.9820–0.9996, showing a good fit with linear function.
(iv) The activation energy *Ea* increases somewhat through the degradation steps revealing the high stability of the remaining part suggesting a high stability of complexes characterized by their covalence.
(v) The negative value of the entropy of activation, ΔS^* of some decomposition steps in case of the ion exchanger and its metal complexes with all investigated metal ions indicates that the activated fragments have more ordered structure than the undecomposed ones and the later are slower than the normal [34,35].
(vi) The positive sign of activation enthalpy change, ΔH^* indicates that the decomposition stages are endothermic processes.
(vii) The high values of the energy of activation, *Ea* of the complexes reveals the high stability of such chelates due to their covalent bond character [36].

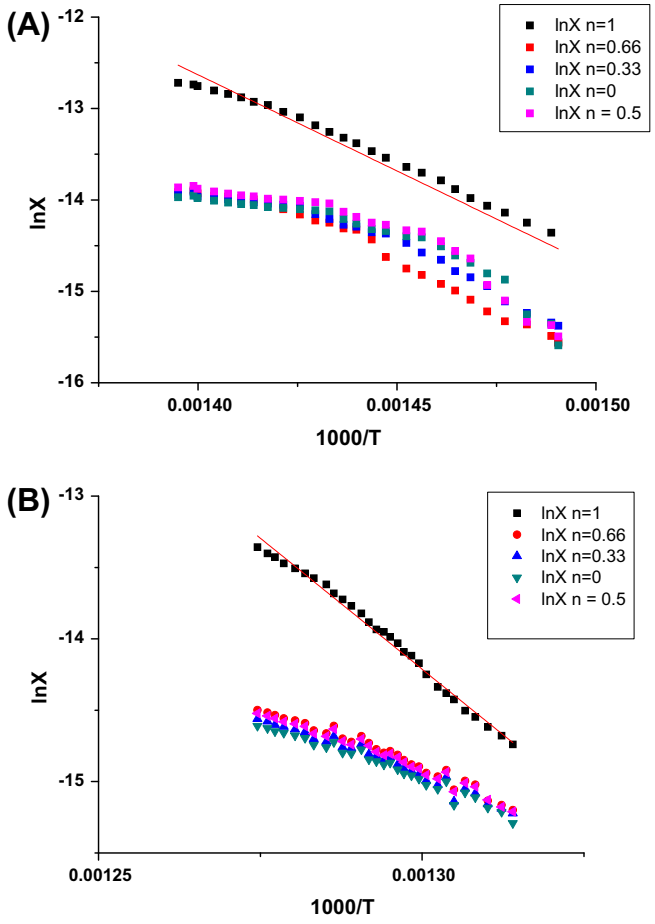

Fig. 1. Coats–Redfern plot of (A) first degradation step and (B) second degradation step for [Co(Ho-HAHNH)$_2$] complex.

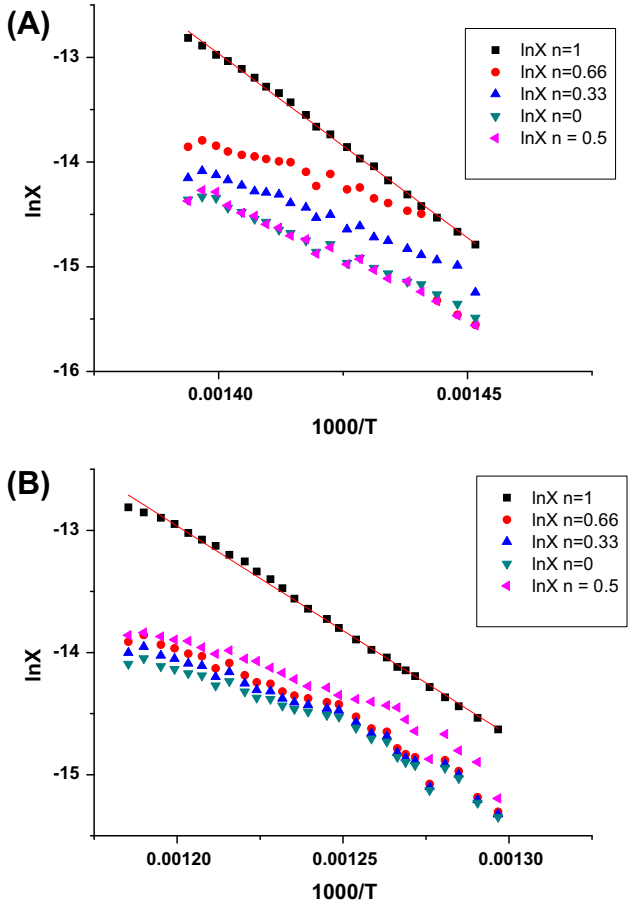

Fig. 2. Coats–Redfern plot of (A) first degradation step and (B) second degradation step for [Cd(Ho-HAHNH)$_2$] complex.

(viii) The positive sign of ΔG^* for the investigated complexes reveals that the free energy of the final residue is higher than that of the initial compound, and hence all the decomposition steps are non-spontaneous processes. This results from increasing the $T\Delta S^*$ clearly from one step to another which override the values of ΔH^* reflecting that the rate of removal of the subsequent species will be lower than that of the precedent one [37–39].

Antifungal activity

In the screening of antifungal activity it has been envisaged that the studies must lead to an overall comparison of activities between the ligand and its metal complex so that the mechanism of the activity can be understood. The experimental antifungal activity data (Fig. 5) indicate that the ligand as well as its complexes shows an appreciable activity against *Aspergillus* sp., *Stemphylium* sp. and *Trichoderma* sp. at 0.5, 1.0 and 1.5 mg/ml concentration. Their activity generally increases with increasing the concentration of the compounds. DMSO control has shown a negligible activity as compare to the ligand and its metal complexes. The complexes are more effective against *Aspergillus* sp. than *Stemphylium* sp. and *Trichoderma* sp. [Cd(Ho-HAHNH)$_2$] shows the highest activity (98%) against *Aspergillus* sp. at the concentration of 1.5 mg/ml among all the metal complexes. The same complex also shows the highest activity (94%) against *Stemphylium* sp. The antifungal activity varies in the following order of fungal species: *Aspergillus* sp. > *Stemphylium* sp. > *Trichoderma* sp. All the metal complexes exhibited greater antifungal activity against *Aspergillus* sp. as compare to the standard drug Miconazole. The Co(II), Cd(II) and U(VI)O$_2$ complexes show better activity against *Stemphylium* sp. than the standard, whereas, Cd(II) complex is more effective against *Trichoderma* sp. From the data it has also been observed that the complexes are more active than the ligand [40]. The toxicity of the complexes can be related to the strength of the metal–ligand bond, besides other factors such as size of the cation [41]. Where, the higher the size of metal ion, the higher the antifungal activity of the complex. Also, the study exhibited that any metal salt alone has higher activity than its investigated complex. However, metal salts alone can not be used as antibacterial agents because of their natural toxicities and the probability of binding to the free ligand [42] presented in the biological systems such as the nitrogen bases of nucleic acids and/or proteins.

The mode of action of the compounds may involve formation of a hydrogen bond through the azomethine group (>C═N–) with the active centers of cell constituents [43,44] resulting in interferences with the normal cell process.

However, this is certain that *o*-Hydroxy acetophenone as well as their metal chelate can offer this novel application if sufficient studies are centered on their biological activities. The present work is a step further in this direction.

Antibacterial activity

The ligand and their metal complexes, standard drug Ampicillin and DMSO solvent control were screened separately for their antibacterial activity against *E. coli* and *Clostridium* sp. at 1.0 and

Table 6
Kinetic Parameters of complexes evaluated by Coats-Redfern equation.

Complex	Peak	Mid Temp (K)	*Ea* (kJ/mol)	A (S^{-1})	ΔH^* (kJ/mol)	ΔS^* (kJ/mol K)	ΔG^* (kJ/mol)
[Co(*Ho*-HAHNH)$_2$]	1st	680	617.98	2.2985E-6	612.32	−0.35970	856.93
	2nd	819	742.71	1.5160E-6	735.90	−0.36471	1034.61
[Cd(*Ho*-HAHNH)$_2$]	1st	670	410.89	2.5196E-6	405.32	−0.35882	645.73
	2nd	837	428.16	9.6590E-7	421.20	−0.36864	729.76

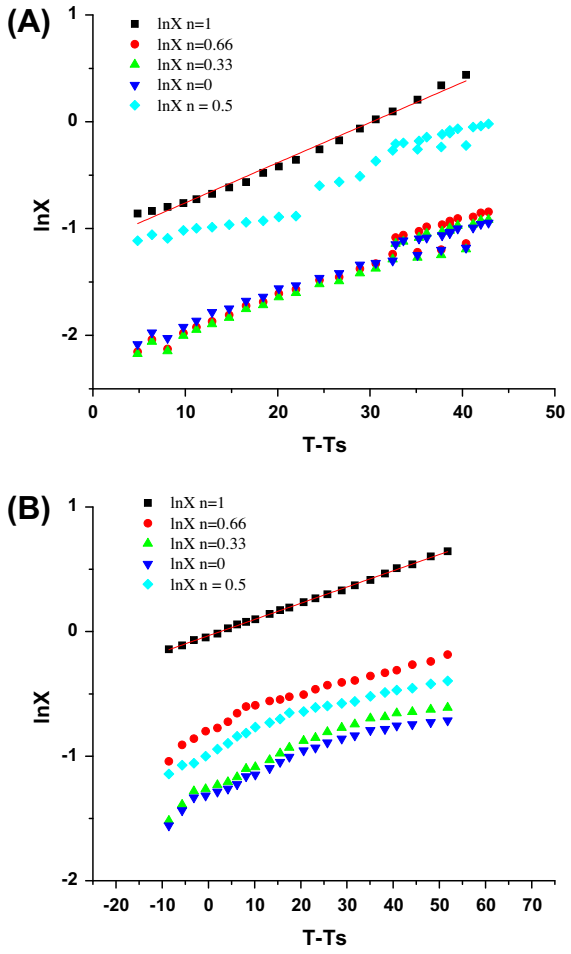

Fig. 3. Horowitz–Metzger plot of (A) first degradation step and (B) second degradation step of [Co(*Ho*-HAHNH)$_2$] complex.

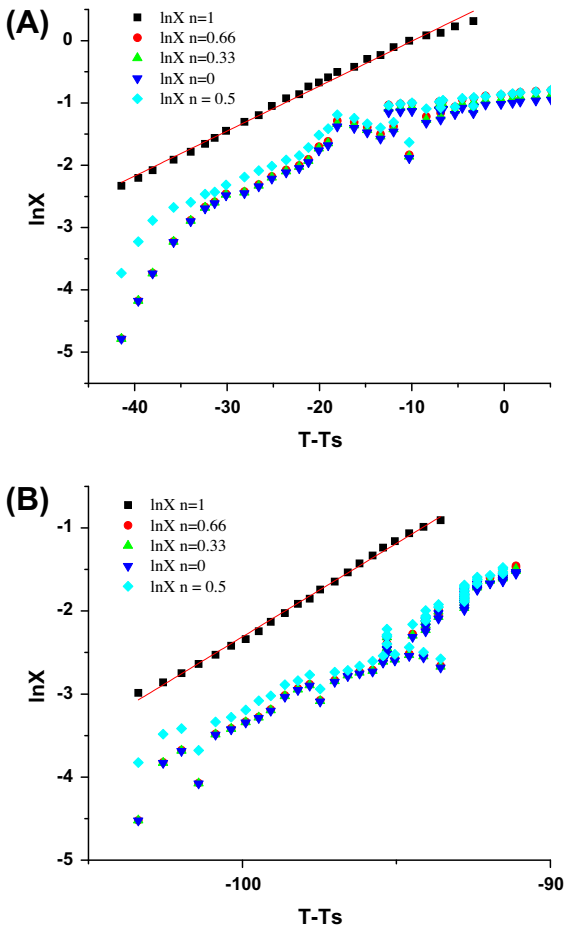

Fig. 4. Horowitz–Metzger plot of (A) first degradation step and (B) second degradation step of [Cd(*Ho*-HAHNH)$_2$] complex.

2.0 mg/ml concentration. Their activity is greatly enhanced at the higher concentration [45]. The activity of the complexes has been compared with the activity of a common standard antibiotic Ampicillin and % Activity Index for the complexes has been calculated. The antibacterial results suggest that the ligand and its complexes (Tables 8 and 9) show a moderate activity against both the bacteria [46,47] as compared to the standard drug (Ampicillin). The metal complexes show higher antibacterial activity than the ligand. The % Activity Index data show the highest activity for [Cd(*Ho*-HAHNH)$_2$] against *E. coli* and *Clostridium* sp. at the concentration of 2.0 mg/ml. The complexes are more effective against *Clostridium* sp. than *E. coli* and show better antibacterial activity than the ligand. According to Overtone's concept of cell permeability, the lipid membrane that surrounds the cell favors the passage of only the lipid-soluble materials due to which liposolubility is an important factor, which controls the antibacterial activity. On chelation, the polarity of the metal ion will be reduced to a greater extent due to the overlap of the ligand orbital and partial sharing of the positive charge of the metal ion with donor groups. Further, it increases

Table 7
Kinetic parameters of complexes evaluated by Horowitz-Metzger equation.

Complex	Peak	Mid Temp (K)	*Ea* (kJ/mol)	*A* (S^{-1})	ΔH^* (kJ/mol)	ΔS^* (kJ/mol K)	ΔG^* (kJ/mol)
[Co(*Ho*-HAHNH)$_2$]	1st	680	617.45	2.1190E-6	611.79	−0.36038	856.86
	2nd	819	742.26	1.4859E-6	735.45	−0.36488	1034.29
[Cd(*Ho*-HAHNH)$_2$]	1st	670	409.45	2.4832E-6	403.88	−0.35894	644.38
	2nd	837	429.73	8.8470E-7	422.78	−0.36937	731.94

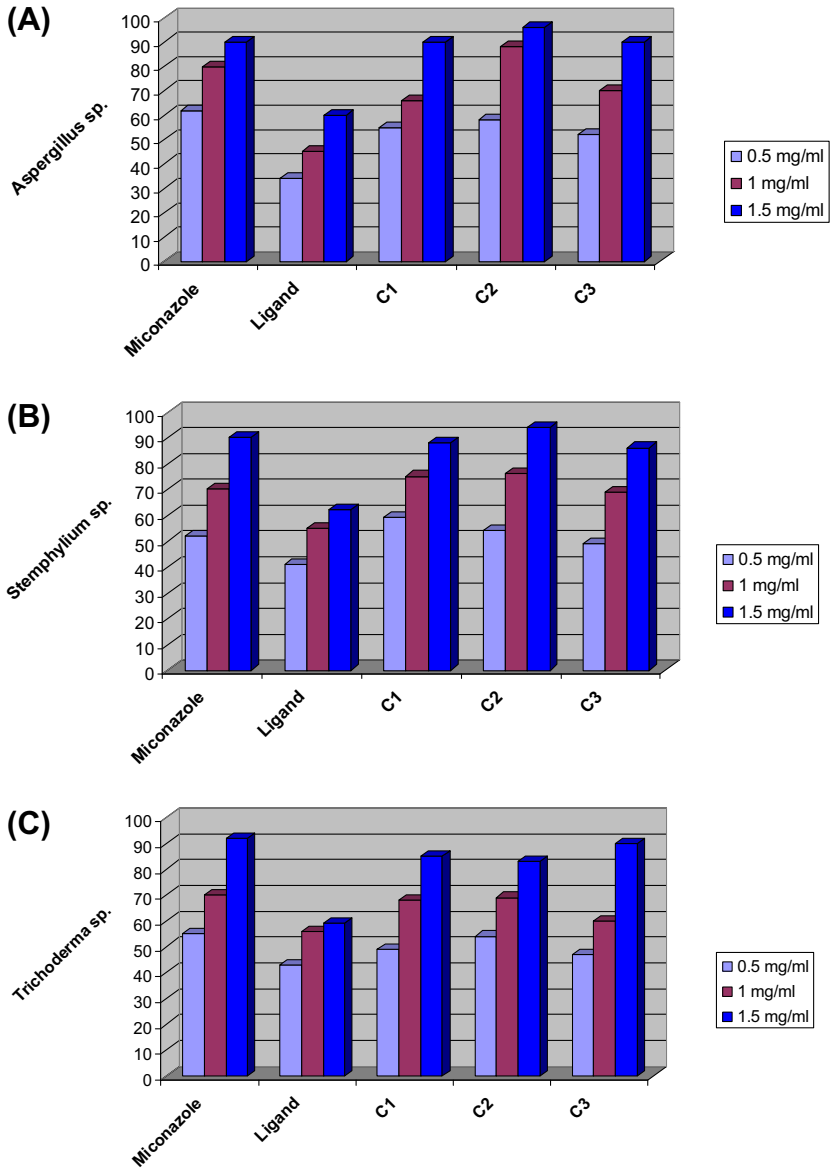

Fig. 5. Effect of ligand and its metal complexes toward (A) *Aspergillus* sp., (B) *Stemphylium* sp. and (C) *Trichoderma* sp.

the delocalization π-electrons over the whole chelate ring and enhances the lipophilicity of the complexes. This increased lipophilicity enhances the penetration of the complexes into lipid membranes and blocking of the metal binding sites in the enzymes of microorganisms. These complexes also disturb the respiration process of the cell and thus block the synthesis of the proteins that restricts further growth of the organism. Furthermore, the mode of action of the compound may involve formation of a hydrogen bond through the azomethine group with the active center of cell constituents, resulting in interference with the normal cell process.

The negative results can be attributed either to the inability of the complexes to diffuse into the Gram-negative bacteria cell membranes and hence unable to interfere with its biological activity or they can diffuse and inactivated by unknown cellular mechanism i.e. bacterial enzymes.

Table 8
Antibacterial activity of the ligand and its complexes.

Compound	*E. coli* (mg/ml)				*Clostridium* sp. (mg/ml)			
	Diameter of inhibition zone (in mm)		% Activity index		Diameter of inhibition zone (in mm)		% Activity index	
	1.0	2.0	1.0	2.0	1.0	2.0	1.0	2.0
H_2o-HAHNH	3	4	19	21	5	7	36	41
[Co(H*o*-HAHNH)$_2$]	15	18	81	84	12	14	86	88
[Cd(H*o*-HAHNH)$_2$]	13	16	81	90	12	16	86	94
[UO_2(H_2o-HAHNH)(OAc)$_2$(H_2O)$_2$]	10	13	63	68	9	12	64	71
Ampicillin	16	19	100	100	14	17	100	100

Table 9
Antimicrobial activitiy in terms of MIC (mg/ml) after 48 h.

Compounds	*E. coli*	*Clostridium* sp.
H_2o-HAHNH	0.8	0.7
[Co(Ho-HAHNH)$_2$]	0.4	0.4
[Cd(Ho-HAHNH)$_2$]	0.4	0.4
[UO_2(H_2o-HAHNH)(OAc)$_2$(H_2O)$_2$]	0.3	0.5
Ampicillin	0.2	0.3

The positive results suggested the very diffusion of the complexes into the bacterial cells and were able to kill the bacterium as indicated by the zones of inhibition of bacterial growth.

References

[1] T.A. Yousef, G.M. Abu El-Reash, T.H. Rakha, U. El-Ayaan, Spectrochim. Acta. 83 (1) (2011) 271–278.
[2] R.R. Zaky, T.A. Yousef, J. Mol. Struct. 1002 (2011) 76–85.
[3] A.S. El-Tabl, F.A. El-Saied, W. Plass, A.N. Al-Hakimi, Spectrochim. Acta, Part A 71 (2008) 90–99.
[4] S. Sivaramaiah, P.A. Reddy, J. Anal. Chem. 60 (2005) 828–832.
[5] A.A. El-Emam, F.F. Belal, M.A. Moustafa, S.M. El-Ashry, D.T. El-Sherbing, S.H. Hansen II, Farmaco 58 (2003) 1179–1186.
[6] M.S. Niasari, A. Amiri, Appl. Catal. 290 (2005) 46–53.
[7] P. Pelagalli, M. Cacelli, C. Pelizz, M. Costa, Inorg. Chim. Acta 342 (2003) 323–326.
[8] M.G. El-Meligy, S.E. El-Rafie, K.M. Abu-Zied, Desalination 173 (2005) 33–44.
[9] K.M. Ibrahim, I.M. Gabr, R.R. Zaky, J. Cood. Chem. 62 (7) (2009) 1100–1116.
[10] K.M. Ibrahim, I.M. Gabr, G.M. Abu El-Reash, R.R. Zaky, Monatsheft. Fur. Chemie. 140 (6) (2009) 625–632.
[11] R.R. Zaky, K.M. Ibrahim, I.M. Gabr, Spectrochim. Acta. 81 (1) (2011) 28–34.
[12] A.I. Vogel, Quantitative Inorganic Analysis, Longmans, London, 1989.
[13] N.L. Allinger, J. Am. Chem. Soc. 99 (1977) 8127–8134.
[14] HyperChem version 8.0 Hypercube, Inc., 2002.
[15] K.M. Ibrahium, T.H. Rakaha, A.M. Abdalla, M.M. Hassanian, J. Ind. Chem. 32 (1993) 361–363.
[16] T.A. Yousef, T.H. Rakha, Usama El Ayaan, G.M. Abu El Reash, J. Mol. Struct. 1007 (2012) 146–157.
[17] T.A. Yousef, O.A. El-Gammal, S.E. Ghazy, G.M. Abu El-Reash, J. Mol. Struct. 1007 (2011) 271–283.
[18] K. Nakamoto, Infrared Spectra of Inorganic, Coordination Compounds, Wiley Interscience, New York, 1970.
[19] K. Pyta, P. Przybylski, A. Huczyński, A. Hoser, K. Wozńiak, W. Schilf, B. Kamieński, D. Eugeniusz Grech, J. Mol. Struct. 970 (2010) 147–154.
[20] D.X. West, D.L. Huffman, J. Trans, Met. Chem. 14 (1989) 190–194.
[21] G.A.A. Al-Hazmiy, M.S. El-Shahawiz, I.M. Gabr, A.A. El-Asmy, J. Coord. Chem. 58 (2005) 713–723.
[22] S.P. McGlynn, J.K. Smith, J. Chem. Phys. 35 (1961) 105–116.
[23] L.H. Jones, Spectrochim. Acta. 10 (1958) 395–403.
[24] M.C. Rodríguez-Argüelles, S. Mosquera-Vázquez, P. Tourón-Touceda, J. Sanmartín-Matalobos, A.M. García-Deibe, M. Belicchi-Ferrari, G. Pelosi, C. Pelizzi, F. Zani, J. Inorg. Biochem. 101 (2007) 138–143.
[25] A.B.P. Lever, Inorganic Electronic Spectroscopy, Elsevier, Amsterdam, 1968.
[26] S. Sagdinc, B. Koksoy, F. Kandemirli, S.H. Bayari, J. Mol. Struct. 917 (2009) 63–70.
[27] A.W. Coats, J.P. Redfern, Nature 20 (1964) 68–69.
[28] H.H. Horowitz, G. Metzger, Anal. Chem. 35 (1963) 1464–1468.
[29] M.S. Abu-Bakr, H. Sedaira, E.Y. Hashem, Talanta 41 (10) (1994) 1669–1674.
[30] D. Kara, M. Alkan, Talanta 55 (2001) 415–423.
[31] A. Broido, J. Ploym. Sci. A-2, 7 (1969) 1761–1773.
[32] K. Schwetlick, Kinetyczne Metody Badania Mechanizmow Reakcji, PWN Warszawa, 1975.
[33] R.G. Mortimer, Physical Chemistry Harcourt and Science Technology Company, Academic Press, San Diego, 2000.
[34] S.H. Guzara, Q.H. Jin, Chem. Res. Chin. Univ. 24 (2) (2008) 143–147.
[35] H.T.S. Britton, Hydrogen Ions, vol. I, third ed., Chapman and Hall, London, 1942.
[36] T. Taakeyama, F.X. Quinn, Thermal Analysis Fundamentals and Applications to Polymer Science, John Wiley and Sons, Chichester, 1994.
[37] P.B. Maravalli, T.R. Goudar, Thermochim. Acta. 335 (1999) 35–41.
[38] K.K.M. Yusuff, R. Sreekala, Thermochim. Acta. 159 (1990) 357–368.
[39] S.S. Kandil, G.B. El-Hefnawy, E.A. Baker, Thermochim. Acta 414 (2004) 105–113.
[40] K.N. Thimmaiah, G.T. Chandrappa, Rangaswamy, Jayarama, Polyhedron 3 (1984) 1237–1239.
[41] R. Nagar, J. Inorg. Biochem. 40 (1990) 349–356.
[42] R.B. Johari, R.C. Sharma, J. Ind. Chem. Soc. 65 (1988) 793–794.
[43] L. Mishra, V.K. Singh, Synth. Ind. J. Chem. 32A (1993) 446–449.
[44] J.R. Soares, T.C.P. Dinis, A.P. Cunha, L.M. Almeida, Free Radical Res. 26 (1997) 469–478.
[45] Z.H. Abd El-Wahab, M.R. El-Sarrag, Spectrochim. Acta. 60A (2004) 271–277.
[46] K. Deepa, K.K. Aravindakshan, Synth. React. Inorg. Met-Org. Nano-Met. Chem. 35 (2005) 409–416.
[47] P.K. Panchal, H.M. Parekh, M.N. Patel, Toxicol. Environ. Chem. 87 (2005) 313–320.